Journal of Corrosion and Materials *J. Corros. Mater.* (2025) 4(1), 33–51.
www.corromat.com

Residue-Cancellation Polynomial Integration for Near-Collision Frozen Calogero–Moser –Sutherland Dynamics

Hisayuki Suematsu[1,*], Charlotte Evans[2]

[1] *Department of Nuclear Technology, Nagaoka University of Technology, Nagaoka, Niigata 940-2188, Japan*

[2] *Department of Mechanical Engineering, TU Dortmund University, 44227 Dortmund, Germany.*

[*] Corresponding author: suematsu@nagaokaut.ac.jp

[2] charlotteevans926@gmail.com

(Received: 31 January 2025. Received in revised form: 22 April 2025. Accepted: 14 May 2025. Published online: 30 June 2025.)

Abstract

Frozen Calogero–Moser–Sutherland dynamics are transformed, in the asymptotic regime of high inverse temperature, into deterministic particle dynamics of reciprocal, boundary, interval, and cotangent type. Near-collision initial conditions make the explicit integration difficult since the particle variables keep their denominators, namely, $(x_i - x_j)^{-1}$ and $(x_i + x_j)^{-1}$, throughout the initial layer of separation. Residue-cancellation-based polynomial integration (RCPI) computes the coefficients of the monic root polynomial instead of computing the singular drift explicitly at each step of integration. The computation is done for the Hermite, Laguerre, compact Jacobi, non-compact Jacobi, and torus cases, employing four six-particle starts at $T = 0.35$ and initial separations down to 4×10^{-4}. The finite-dimensional system of coefficients arises from the inverse heat, inverse Bessel-heat, inverse Jacobi-type, and torus operators. The roots are validated by maximum root discrepancy, closure residual, radial growth, interval confinement, and circular spacing. In the case of the Hermite, Laguerre, compact Jacobi, and torus computations, the discrepancy of the final roots from the direct singular ODE integration falls between 5.11×10^{-15} and 3.06×10^{-14} while the evaluations of the right-hand side have been saved by a factor ranging from 3.02 to 23.80. The values demonstrate that the potential near-collision singularity is stripped away from the time integration process once the residue cancellation is stated in terms of the polynomial coefficients.

Keywords: Calogero–Moser–Sutherland systems; root polynomial dynamics; freezing limits; inverse heat operators; coefficient propagation; near-collision

1. Introduction

Calogero–Moser–Sutherland dynamics represent one of the conventional links between exactly solvable many-body systems, eigenvalue motions of random matrices, Dunkl analysis, and multivariate special functions. Calogero derived one classical integrable many-body system [1]. The structure of Sutherland was developed for the corresponding one-dimensional quantum many-body system [2]. Dyson constructed one stochastic eigenvalue process where repulsion prevents collisions [3]. Further, the stochastic analysis of interacting Brownian particles made the connection with the limiting behavior of random matrices [4]. Dunkl discovered the differential-difference operators with respect to reflection groups [5]. Special Hermite polynomials made the connection between these operators and heat equations [6]. The corresponding Markov processes provided the connection with stochastic processes related to the corresponding Dunkl operators [7]. Subsequently, the Dunkl process was defined on root systems [8]. The log-gas theory provided the unification of these interacting particles within the framework of the beta ensemble [9]. The Bessel process theory additionally provided the link of the Dyson model with non-collision diffusion [10]. In the Laguerre family, eigenvalues could be represented by non-collision squared Bessel processes [11]. Beta Jacobi processes represent the corresponding compact interval diffusion processes [12]. The theory of random matrices puts the examples like Wishart and MANOVA into one framework of eigenvalues [13].

The freezing limit extracts the deterministic skeleton of these models. The analysis of type-A interacting particles directly connected the Dunkl intertwining and the freezing behavior [14]. Another work discovered two limiting regimes of interacting Bessel processes [15]. After appropriate scaling according to the inverse temperature parameter, the Brownian part disappeared and the limiting trajectories were governed by a singular ordinary differential equation on an ordered chamber, half-line chamber, compact interval, non-compact chamber, or circle. The appearance of these singular terms was not accidental. It encoded the collision prevention, the repulsion at endpoints, and the circular spacing. The electrostatic repulsion systems provide the results of existence of interacting diffusions [16]. The strong solution theory provides the non-collision property for many particle systems [17]. The freezing differential equations of CMS have been analyzed in the root system families [18]. The unified approach also reveals the corresponding special solutions and their orthogonal polynomial zeros [19]. The Hermite and Laguerre ensembles have explicit asymptotics in large β [20]. The multivariate Bessel processes are governed by limit theorems in the freezing regime [21]. Central limit theorems also provide the information about the fluctuations of high inverse temperature [22]. The polynomial martingales encode observables that remain consistent with these limits [23]. The Jacobi processes have also the Wigner- and Marchenko–Pastur-type limits [24]. Generally, the CMS particle models allow a unified framework of their limits in several geometries [25].

The near-collision initiates the direct ODE solver with the first task of resolving an initial repulsion layer caused by $(x_i - x_j)^{-1}$, $(x_i + x_j)^{-1}$, $(1 - x_i x_j)/(x_i - x_j)$, and $\cot((x_i - x_j)/2)$. The exact trajectory goes immediately into the interior, but the particle coordinate formula keeps revealing the solver to singular denominators. The calculation below uses the vector of coefficients of the root polynomial as the time-dependent variable and tests whether the obtained roots coincide with the direct integration of singularities while keeping the identities inherent to each model.

The residue-cancelled polynomial integration, shortly RCPI, maps the coefficients of the monic polynomial having the zeros equal to the particles. The inverse heat equation in the Hermite case, the inverse Bessel-heat equation in the Laguerre case, the inverse Jacobi-type equations in the compact and non-compact cases, and the diagonal torus coefficient equation all keep the degree of the polynomials constant. Therefore, the polynomial equation becomes the finite-coefficient system. The root extraction is done at observation times and checked by the closure residual, the exact radial identity, the interval containment, and the circular spacing.

The four deterministic six-particle starts are advanced to $T = 0.35$. They are not equilibrium configurations. The Hermite, Laguerre, compact Jacobi, and torus starts have the minimum initial separation of 5×10^{-4}, 4×10^{-4}, 5×10^{-4}, and 10^{-3}, respectively. These numbers put the direct particle equations in the most expensive early-time regime while keeping all the initial coordinates, final roots, residuals, and invariant checks reportable in full.

The construction presented in Figure 1 follows the actual calculation: ordered particles define model-specific monic polynomials, their coefficients evolve under the inverse operators, and final particle positions are obtained via root extraction.

The singular pairwise terms are missing during the coefficient integration and appear only via the recovered roots.

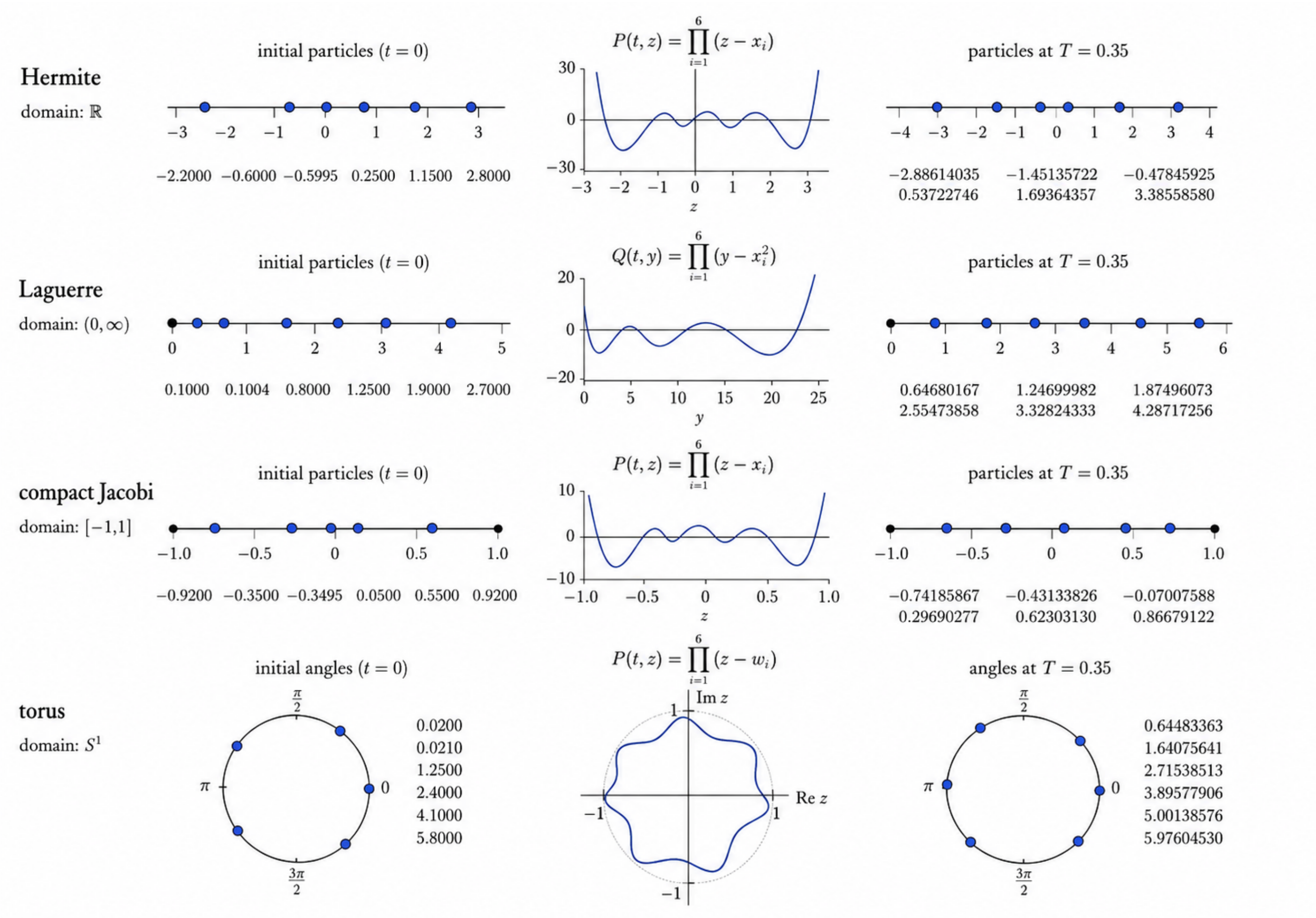

Figure 1: Root-polynomial encoding used by coefficient propagation.

The panel of Figure 1 keeps the three objects used throughout the calculation: the ordered particle vector, the monic polynomial, and the recovered root set. The endpoint comparison at $T = 0.35$ tests the numerical root recovery rather than a symbolic identity alone.

The polynomial relations used here are based on the classical zero characterization of Hermite, Laguerre, and Jacobi families [26]. The inverse heat-type identities and the frozen CMS equations provide the corresponding coefficient flows [19]. This calculation gives the accuracy of roots, operator residuals, configuration results, and invariants for explicitly specified near-collision cases, thus checking the correctness of the polynomial root assignment numerically.

2. Frozen CMS equations and polynomial operators

The construction uses five frozen particle families. The Hermite model is posed on the type-A Weyl chamber

$$C_N^A = \{x \in \mathbb{R}^N : x_1 \le x_2 \le \cdots \le x_N\} \tag{1}$$

and is governed by

$$\dot{x}_i(t) = \sum_{j \ne i} \frac{1}{x_i(t) - x_j(t)}, \qquad i = 1, \dots, N. \tag{2}$$

It is the deterministic freezing limit of Dyson-like Brownian motion with the inverse temperature scaling having already stripped off the stochastic component. The unique self-similar solution is $x(t) = \sqrt{2t}\, z$, where $z_1 < \cdots < z_N$ are the ordered roots of the Hermite polynomial H_N. The quadratic relation

$$\|x(t)\|^2 = N(N-1)t + \|x(0)\|^2 \tag{3}$$

offers an immediate verification of computed orbits. In the centered case, convergence to the Hermite root solution occurs after a normalizing map in terms of time-dependent radius and exponential contraction in angular variables. The stability view point is in line with the usual dynamical systems analysis of flows close to attractive fixed points [27]. This is one major justification of using the Hermite model as a good example for testing desingularized coefficient propagation.

The Laguerre model is posed on the type-B chamber

$$C_N^B = \{x \in \mathbb{R}^N : 0 \le x_1 \le x_2 \le \cdots \le x_N\} \tag{4}$$

and contains both pairwise repulsion and boundary repulsion at zero:

$$\dot{x}_i(t) = \sum_{j \ne i} \left(\frac{1}{x_i(t) - x_j(t)} + \frac{1}{x_i(t) + x_j(t)} \right) + \frac{\nu}{x_i(t)}, \qquad \nu > 0. \tag{5}$$

The special self-similar solution is obtained from the ordered zeros of $L_N^{(\nu-1)}$: if $z_1^{(\nu-1)} \le \cdots \le z_N^{(\nu-1)}$ are these zeros and $y_i^2 = z_i^{(\nu-1)}$, then $x(t) = \sqrt{2t}\, y$ solves the frozen Laguerre equation. The norm identity

$$\|x(t)\|^2 = 2N(N+\nu-1)t + \|x(0)\|^2 \tag{6}$$

plays an identical diagnostic function to equation (3). It is crucial that there be a square of the variable; otherwise, the polynomial form is unstable for $y = x^2$ and transforms the singularity at the boundary into a coefficient transport term.

The compact Jacobi model is posed on

$$A_N = \{x \in \mathbb{R}^N : -1 \le x_1 \le x_2 \le \cdots \le x_N \le 1\} \tag{7}$$

with parameters $p, q > N - 1$ and drift

$$\dot{x}_i(t) = (p-q) - (p+q)x_i(t) + 2\sum_{j \ne i} \frac{1 - x_i(t)x_j(t)}{x_i(t) - x_j(t)}. \tag{8}$$

The stationary point is the vector of zeros of the Jacobi polynomial $P_N^{(q-N,p-N)}$ on $[-1, 1]$. In contrast to the Hermite and Laguerre models, the compact model is asymptotically stationary, not self-similar. A convenient coordinate transform is $x_i = \cos \tau_i$, under which the dynamics becomes a gradient system in trigonometric coordinates. The speed of convergence in those coordinates is determined by

$$c = \frac{p + q + 2\min(p, q) + 2 - 2N}{4}, \tag{9}$$

which is positive with respect to the given condition on parameters. This is a weaker computational criterion compared to the triangular coefficients of the Hermite and Laguerre expansions, but it is crucial from the point of interpretation of the asymptotic compactness of the Jacobi expansion.

The non-compact Jacobi expansion is related to Jacobi polynomials and hypergeometric functions corresponding to root systems [28]. Stochastic counterpart of the Jacobi expansion is a member of Heckman–Opdam Markov processes family [29]. The expansion is defined on

$$C_N = \{x \in \mathbb{R}^N : 1 \le x_1 \le x_2 \le \cdots \le x_N\} \tag{10}$$

and is governed by

$$\dot{x}_i(t) = (q-p) + (q+p)x_i(t) + 2\sum_{j\neq i} \frac{x_i(t)x_j(t) - 1}{x_i(t) - x_j(t)}. \tag{11}$$

Due to its algebraic similarity with the compact Jacobi drift, the model under discussion is also applicable to the coefficient-operator technique. However, the asymptotic dynamics of the system is distinguished by the fact that, unlike the compact system, the non-compact model is characterized by hyperbolic growth.

The torus model is most naturally stated in angular variables on

$$C_N = \{x \in \mathbb{R}^N : x_1 \le x_2 \le \cdots \le x_N \le x_1 + 2\pi\}, \tag{12}$$

where the frozen equation is

$$\dot{x}_j(t) = \sum_{l\neq j} \cot\left(\frac{x_j(t) - x_l(t)}{2}\right). \tag{13}$$

For polynomial transport it is preferable to use $w_j(t) = \mathrm{e}^{\mathrm{i}x_j(t)}$. Then the equation becomes

$$\dot{w}_j(t) = -(N-1)w_j(t) - 2\sum_{l\neq j} \frac{w_j(t)w_l(t)}{w_j(t) - w_l(t)}. \tag{14}$$

Stochastic models for such a periodic structure are formed by non-intersecting Brownian motions on the circle [30]. Angular momentum is preserved, and all trajectories evolve to the same equally spaced arrangement of particles on the circle with equal angular momentum center. The contraction estimate

$$\|x(t) - \widetilde{x}(t)\| \le \mathrm{e}^{-Nt/2} \|x(0) - \widetilde{x}(0)\| \tag{15}$$

holds for solutions with identical angular sums, after the natural chamber convention is fixed.

Table 1: Frozen equations and polynomial operators.

Model	Domain	Polynomial representation	Operator equation
Hermite	$C_N^A \subset \mathbb{R}^N$	$P(t,z) = \prod_{i=1}^N (z - x_i(t))$	$P_t = -\frac{1}{2}P_{zz}$
Laguerre	$C_N^B \subset [0,\infty)^N$	$P(t,z) = \prod_{i=1}^N (z^2 - x_i(t)^2)$	$P_t = -\left(\frac{1}{2}P_{zz} + \frac{\nu-1/2}{z}P_z\right)$
Compact Jacobi	$A_N \subset [-1,1]^N$	$P(t,z) = \prod_{i=1}^N (z - x_i(t))$	$P_t = -\{(1-z^2)P_{zz} + [(p-q) + (2N-2-p-q)z]P_z\} - N(p+q-N+1)P$
Non-compact Jacobi	$C_N \subset [1,\infty)^N$	$P(t,z) = \prod_{i=1}^N (z - x_i(t))$	$P_t = -\{(z^2-1)P_{zz} + [(2N-2-p-q)z - (q-p)]P_z\} + N(p+q-N+1)P$
Torus	$w_j \in \mathbb{T}$	$P(t,z) = \prod_{j=1}^N (z - w_j(t))$	$P_t = z^2 P_{zz} - (N-1)zP_z$

The operator parameters listed in Table 1 define the full computational problem. In each line of the table, both the singular particle differential equation and the polynomial of fixed degree that is used for time evolution are specified. This double specification ensures clarity in whether drift terms are kept or dropped, including the Laguerre boundary, Jacobi compact potential, and diagonal torus action terms.

3. Coefficient integration for residue cancellation

Let $P(t,z)$ be a monic polynomial of degree N where the zeros represent the particle state. The desingularization technique relies on the coefficient vector

$$P(t,z) = \sum_{m=0}^{N} a_m(t) z^m, \qquad a_N(t) = 1. \tag{16}$$

Instead of solving the singular particle ODE directly, RCPI solves

$$\frac{\mathrm{d}}{\mathrm{d}t} a(t) = M_\theta a(t), \tag{17}$$

with M_θ being the finite-dimensional linear coefficient operator arising from the appropriate polynomial operator and θ being the model parameters. The particle configuration is found by root finding only after the coefficients have been evolved using the flow equation. Because (17) is a linear and finite-dimensional equation, the process may be understood as the evolution of the initial polynomial under the semigroup e^{tM_θ}.

For the Hermite model, substituting (16) into $P_t = -\frac{1}{2}P_{zz}$ yields

$$a'_m(t) = -\frac{1}{2}(m+2)(m+1)a_{m+2}(t), \qquad 0 \le m \le N-2, \tag{18}$$

with $a'_{N-1}(t) = a'_N(t) = 0$. This is a two-step recurrence that is triangular in the monomial basis. The triangular structure accounts for the reason why Hermite test uses few coefficients to evaluate. With exact computation, the coefficient of z^m depends only on coefficients of the same parity and with higher degree, with the leading coefficient being fixed.

In the case of the Laguerre scheme, the variable that ensures stability of coefficients is $y = z^2$. Let

$$Q(t,y) = \prod_{i=1}^{N}(y - x_i(t)^2) = \sum_{m=0}^{N} b_m(t)y^m, \tag{19}$$

the inverse Bessel-heat equation becomes

$$Q_t = -2yQ_{yy} - 2\nu Q_y. \tag{20}$$

The coefficient flow is therefore

$$b'_m(t) = -2(m+1)(m+\nu)b_{m+1}(t), \qquad 0 \le m \le N-1, \tag{21}$$

with $b'_N(t) = 0$. The system is triangular with one step, and the parameter ν occurs as a simple multiplier of linear coefficients only. Such formulation is especially handy when checking sensitivity to the repulsion from zero.

For the compact Jacobi scheme, define

$$A = p - q, \qquad B = 2(N-1) - (p+q), \qquad C = N(p+q-N+1). \tag{22}$$

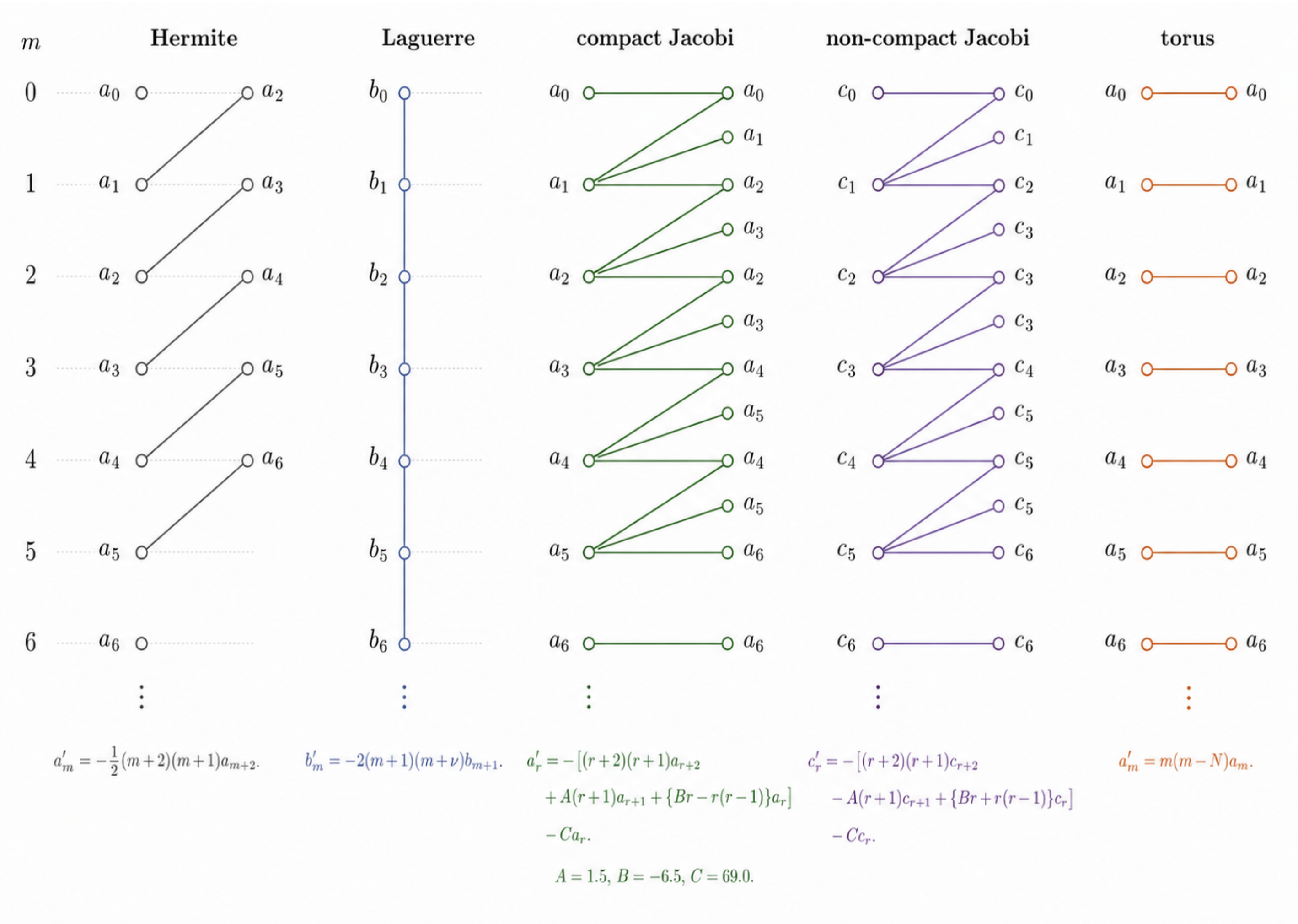

Figure 2: Polynomial coefficient couplings.

The coefficient flow generated by the compact Jacobi operator is

$$a'_r(t) = -\left[(r+2)(r+1)a_{r+2}(t) + A(r+1)a_{r+1}(t) + \{Br - r(r-1)\}a_r(t)\right] - Ca_r(t), \tag{23}$$

provided that $a_s(t) = 0$ for $s > N$. The system is not triangular but banded due to the interaction of second derivatives, first derivatives, multiplication by z, and the potential part. However, the top coefficient is a constant since the coefficient in front of a_N is zero. This cancellation is an essential algebraic condition: without it, the polynomial degree would not be preserved and the root representation would not stay within a fixed particle number.

For the non-compact Jacobi model, the same construction gives the sign-adjusted coefficient flow

$$a'_r(t) = (r+2)(r+1)a_{r+2}(t) + (q-p)(r+1)a_{r+1}(t) - \{r(r-1) + Br\}a_r(t) + Ca_r(t), \tag{24}$$

with missing coefficients being treated as zeros. This equation is presented since the case of the non-compact set falls under the same algebraic framework, even though the numerical computations which follow concentrate on the Hermite, Laguerre, compact Jacobi, and torus cases, where comparison with reference behavior is more obvious.

For the torus equation in w-coordinates, the coefficient flow is diagonal:

$$a'_m(t) = m(m-N)a_m(t), \qquad 0 \le m \le N. \tag{25}$$

Consequently, each elementary symmetric coefficient is scaled by a simple exponential term. This diagonal scaling pattern gives the torus model the most elegant coefficient transfer structure of all, despite requiring delicate circular angle matching for root recovery along the unit circle.

The finite-dimensional operator structure is illustrated in Figure 2. This figure distinguishes between the two-step Hermite recursion, the one-step Laguerre recursion in the squared variable, the banded Jacobi coefficient system (both compact and non-compact), and the torus flow (diagonal). These structures explain why the time integration can be done without singular pairwise denominators.

The coefficient atlas in Figure 2 will explain the ranking found in the computational cost results below. Triangular sparse transport should have low costs; banded Jacobi transport will be more costly; and torus transport localizes the angular singularity into a single coefficient factor.

Proposition 3.1. *The equivalence between coefficient transport and particle motion If $P(t,z)$ is a monic polynomial with distinct roots in the relevant chamber, alcove, half-line chamber, non-compact chamber, or torus coordinate space, and P solves the relevant operator equation in Table 1, then the roots solve the relevant frozen particle equation. Moreover, if there exists a smooth interior solution of the particle equation, then the polynomial with these roots solves the operator equation.*

Proof. The proof is a residue-cancellation argument. In the Hermite, compact Jacobi, and non-compact Jacobi cases write $P(t,z) = \prod_{i=1}^{N}(z - x_i(t))$ and $P_i(t,z) = P(t,z)/(z - x_i(t))$. Since $P(t, x_i(t)) = 0$, differentiation gives

$$0 = P_t(t, x_i(t)) + P_z(t, x_i(t))\dot{x}_i(t), \tag{26}$$

and therefore $\dot{x}_i(t) = -P_t(t, x_i(t))/P_z(t, x_i(t))$. Substituting the operator equation for P_t reduces this quotient to a logarithmic derivative of P_i at the root. The identity

$$\frac{P'_i(t, x_i(t))}{P_i(t, x_i(t))} = \sum_{j \neq i} \frac{1}{x_i(t) - x_j(t)} \tag{27}$$

and then obtains the repulsion term. The terms involving the Jacobi functions $(1 - x_i^2)$ and $(x_i^2 - 1)$ can be greatly simplified due to the fact that $1 - x_i^2$ or $x_i x_j - 1$ is related to $1 - x_i x_j$ via algebraic identities. The result for the Laguerre polynomials comes out from the same considerations, when one considers the function $Q(t,y) = \prod_{i=1}^{N}(y - x_i(t)^2)$ and takes the logarithmic derivative in the square variable. For the torus one simply substitutes $x_i \to w_i = e^{ix_i}$ in the formula and applies the same cancellation to $P(t,z) = \prod_j (z - w_j(t))$. The converse implication is obtained by differentiating the product formula for the polynomial and reversing the calculation. □

The calculation of RCPI turns the initial values into monic polynomial coefficients, advances them via the linear system from the model, and computes the final roots. Line and interval roots are sorted by their real values, while torus roots are transformed into angles in the range $[0, 2\pi)$ and matched under rotations. Root extraction of high-degree polynomials can still be ill-conditioned, but not the reciprocal and cotangent drifts anymore.

To monitor consistency, the study uses the normalized closure residual

$$\mathcal{R}_M(t) = \max_{\zeta \in \Xi_M} \frac{|P_t(t,\zeta) - \mathcal{L}_\theta P(t,\zeta)|}{1 + |P_t(t,\zeta)| + |\mathcal{L}_\theta P(t,\zeta)|}, \tag{28}$$

where Ξ_M is the given set of complex collocation points and $\mathcal{L}_\theta$ is the operator involved. When the coefficients are solved exactly, the operator residual is zero. In the floating-point case, it reflects how well the coefficient vector solves the polynomial operator equation at machine precision. It is separate from root error since a small operator residual is not sufficient to ensure accurate recovery of all polynomial zeros for large N.

4. Algebraic and geometric checks

Not only numerical consistency at a fixed point can serve as a criterion for validity of the coefficient method. It is necessary to confirm that the desingularized representation satisfies all algebraic and asymptotic invariants characteristic of the particle system. The Hermite norm identity (3) and the Laguerre norm identity (6) provide an analytic check since they impose the exact law of growth of the squared radius of a Euclidean ball. By applying the corresponding identity after root extraction, one may compare the obtained value with the formula for the initial state. The value of such check is that it tests simultaneously the coefficient evolution algorithm and the root extraction step. If the former is implemented correctly but the latter produces a cluster of roots belonging to some wrong branch, the check will probably reveal the discrepancy.

For the compact Jacobi system, the test does not concern the radial growth but is related to the confinement and attraction properties. The polynomial roots have to stay within the interval $[-1,1]$, maintain their order after sorting and converge towards the stationary Jacobi-zero configuration corresponding to $P_N^{(q-N,p-N)}$. This gives the threefold analytical test: boundedness in the compact alcove, positive separation for $t > 0$ and decreasing distance to the stationary Jacobi-zero vector in the trigonometric metric defined by $x_i = \cos\tau_i$. The potential term cannot be dropped from the coefficient operator since the degree of the polynomial stays N and the root process takes place in the compact interval. The removal of that term is not an insignificant simplification but leads to violation of the finite-dimensional closure and the relation between root motion and inverse Jacobi heat flow.

The verification process in case of the torus system is cyclic rather than linear. The roots of the polynomial have to stay near the unit circle, the angular barycentre has to be preserved modulo 2π and the separations have to get close to the equal spacing. The root extraction process has to be done using the circular matching rather than the usual sorted Euclidean matching. The exponential contraction formula (15) indicates that the near collision pair has to separate quickly, and the state will become a regular polygon afterwards. The coefficient method that reproduces the solution but loses the unity modulus will be algebraically wrong; in the computed final state, the angular root state will be correct with respect to the torus geometry.

The determinantal identity provides the second check. It proves that the very same polynomial propagating under RCPI is the polynomial entering the expectation formulas for normalized multivariate Bessel and Jacobi processes. This is important because the frozen ODEs are not the independent systems but the limiting skeletons of certain stochastic processes. Even if a numerical method computes the trajectory of the system, it does not guarantee the preservation of the observable polynomial that enters the martingale identities. The coefficient propagation method is immune to that since it exactly propagates the polynomial solution entering the expectation identities.

The checks are based on explicit formulas. The Hermite and Laguerre identities prescribe the law of radial growth; the compact Jacobi operator imposes the interval confinement and the potential term; the non-compact Jacobi operator imposes the sign change and the hyperbolic chamber; and the torus equation prescribes the circular ordering and angular barycentre. The results presented in this paper can be obtained from these formulas and the initial data in Table 2.

5. Six-particle starts at $T = 0.35$

Each run uses $N = 6$ particles and end time $T = 0.35$. The initial conditions are characterized by either a small separation or near-boundary condition. For Hermite, there are two line particles separated by 5×10^{-4}. For Laguerre, there are two positive particles separated by 4×10^{-4} near the reflecting boundary at zero. For the compact Jacobi, there is a near-collision inside $[-1,1]$ along with near boundary particles. In the torus case, there are two angles separated by 10^{-3} on the circle.

Both the coefficient equation and the direct particle equation are solved using a high-order adaptive Runge–Kutta integrator with relative tolerance 10^{-12} and absolute tolerance 10^{-14}. This comparison is made using three values. First, there is the maximum root discrepancy at the final time,

$$E_\infty(T) = \max_i |x_i^{\mathsf{RCPI}}(T) - x_i^{\mathrm{ODE}}(T)|, \tag{29}$$

using circular angle matching for the torus case. Second, there is the final minimum separation, which shows that the final configuration is an interior configuration. Third, there is the number of right-hand-side evaluations needed by the adaptive integrator. Since the coefficient equations are linear and non-singular, they are expected to need fewer evaluations, but the degree of the reduction will depend on the band structure of the coefficient operator and the root configuration.

The coordinates in Table 2 are fixed deterministic starts, with small distances making the direct particle solver calculate singular drifts terms while RCPI calculates a nonsingular coefficient vector.

The arrangement of Figures 3 contains the same coordinates but in their natural domain. The panels with lines, half-lines, intervals, and circles demonstrate the initially close pairs and their separated endpoint states as a result of coefficient transport.

Table 2: Near-collision starts.

Model	Parameters	Initial configuration
Hermite	$N = 6,\ T = 0.35$	$(-2.2000, -0.6000, -0.5995, 0.2500, 1.1500, 2.8000)$
Laguerre	$N = 6,\ \nu = 1.75,\ T = 0.35$	$(0.1000, 0.1004, 0.8000, 1.2500, 1.9000, 2.7000)$
Compact Jacobi	$N = 6,\ p = 9.0,\ q = 7.5,\ T = 0.35$	$(-0.9200, -0.3500, -0.3495, 0.0500, 0.5500, 0.9200)$
Torus	$N = 6,\ T = 0.35$	Angular state $(0.0200, 0.0210, 1.2500, 2.4000, 4.1000, 5.8000)$

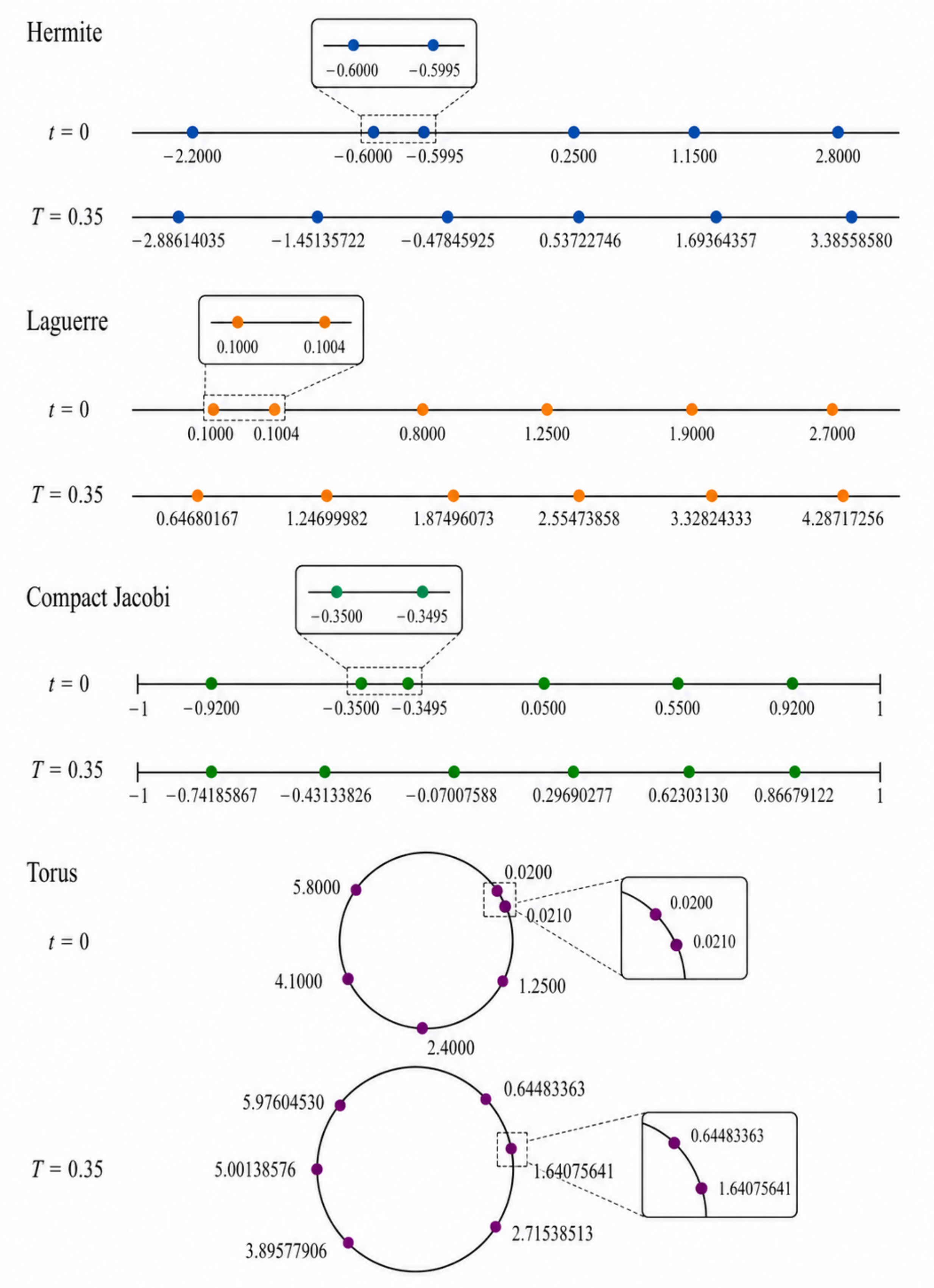

Figure 3: Initial and final particle locations.

Location diagram in Figure 3 explains geometric sense of the four starts where the endpoint states are separated chambers, half-line, interval, and circular geometries derived from corresponding coefficient equations.

6. Final roots, residuals, and solver effort

The key numerical results are reported in Table 3. Coefficient propagation matches singular ODE integration with nearly machine precision for all considered tests. The maximum final absolute differences between the two approaches amount to 7.22×10^{-15} for the Hermite test, 3.06×10^{-14} for the Laguerre test, 5.11×10^{-15} for the compact Jacobi test, and 1.42×10^{-14} for the torus test. The error is much smaller than the tolerances of time-integration procedure since both methods calculate smooth interior dynamics for most of the interval and since the coefficient equations are exact equivalents of particle equations.

Table 3: Final accuracy and solver cost.

Model	RCPI evaluations	Direct evaluations	Evaluation ratio	$E_\infty(T)$	$\Delta_{\min}(T)$
Hermite	50	1190	23.80	7.22×10^{-15}	0.9728979702
Laguerre	230	1406	6.11	3.06×10^{-14}	0.6001981443
Compact Jacobi	482	1454	3.02	5.11×10^{-15}	0.2437599247
Torus	206	1466	7.12	1.42×10^{-14}	0.9519736399

The values in Table 3 provide an explicit measure of the comparison between the coefficient integral and the singular particle integral. The final root errors are all still round-off, but in this case, the direct ODE solver evaluates between three and nearly twenty-four times as many right-hand-sides. These ratios correspond to the structure of the operators: Triangular Hermite transport is least expensive, Jacobi banding is more expensive, and diagonal torus transport does not have coupling between coefficients.

The particle trajectories in Figure 4 show the smooth separation of the initial near-collision pairs with the correct relative order or circular convention maintained. The cost/error ledger in Figure 5 plots the right-hand-side evaluation counts against the final root errors, confirming that the use of fewer drift evaluations does not come at the expense of increased root error.

Thus, together, the trajectory and cost plot in Figures 4 and 5 demonstrate the relation between the qualitative and quantitative results. The roots separate smoothly according to the geometry provided by the model, and the cost plot demonstrates that the separation can be achieved without incurring the total cost of repeated drift evaluations.

The Hermite result is the clearest demonstration of desingularization. The direct integrator must initially resolve the separation of the near-collision pair at -0.6000 and -0.5995, since the singularity of the denominator causes the drift to be very large in this region. The coefficient equation, on the other hand, simply transports the coefficients in accordance with the triangular recurrence (18). Thus, in this example, it requires only 50 right-hand-side evaluations compared with the direct ODE integrator which requires 1190 right-hand-side evaluations. At $T = 0.35$, the recovered configuration is

$$(-2.88614035, -1.45135722, -0.47845925, 0.53722746, 1.69364357, 3.38558580). \tag{30}$$

The separation between the third and fourth particles is now large enough that it no longer has a small separation. The solution has thus been transported off the near collision boundary, and the coefficient flow achieves this transportation without ever evaluating a singular reciprocal.

The Laguerre result is the most dramatic illustration of the benefit of using the squared variable. Direct evaluation in terms of z while the configuration is near zero would lead to polynomials with symmetrical root pairs and poor conditioning. However, in terms of $y = x^2$, the coefficient equation (21) becomes one-step triangular, containing only the term $m + \nu$ in the boundary parameter ν. The recovered positive configuration is

$$(0.64680167, 1.24699982, 1.87496073, 2.55473858, 3.32824333, 4.28717256). \tag{31}$$

In this case, the near-boundary pair has been separated from an initial position of 0.1000 and 0.1004 to a separated interior pair with a final minimum separation of 0.6001981443. The direct solver required 1406 right-hand-side evaluations, whereas RCPI required 230. The evaluation ratio of 6.11 is smaller than that for the Hermite example, but this is due to the faster growth of the coefficients in (21) and the additional nonlinear step of root recovery in terms of squared variables, but the reduction is still significant.

The compact Jacobi experiment is more difficult because the coefficient equation is a band matrix equation with potential and endpoint effects. This system features a near-collision pair, along with particles near -1 and 1. The recovered configuration is

$$(-0.74185867, -0.43133826, -0.07007588, 0.29690277, 0.62303130, 0.86679122). \tag{32}$$

The final coefficients are kept within the small alcove, and the minimum distance is 0.2437599247. It is lesser compared to the previous experiment because of the compactness of the interval and attraction to the stationary distribution of Jacobi zeros. The direct solver needs 1454 evaluations of right-hand side vectors, while RCPI needs 482. The ratio of evaluations is 3.02, which is quite good but at the same time means that Jacobi coefficients are not as sparse as Hermite and Laguerre coefficients.

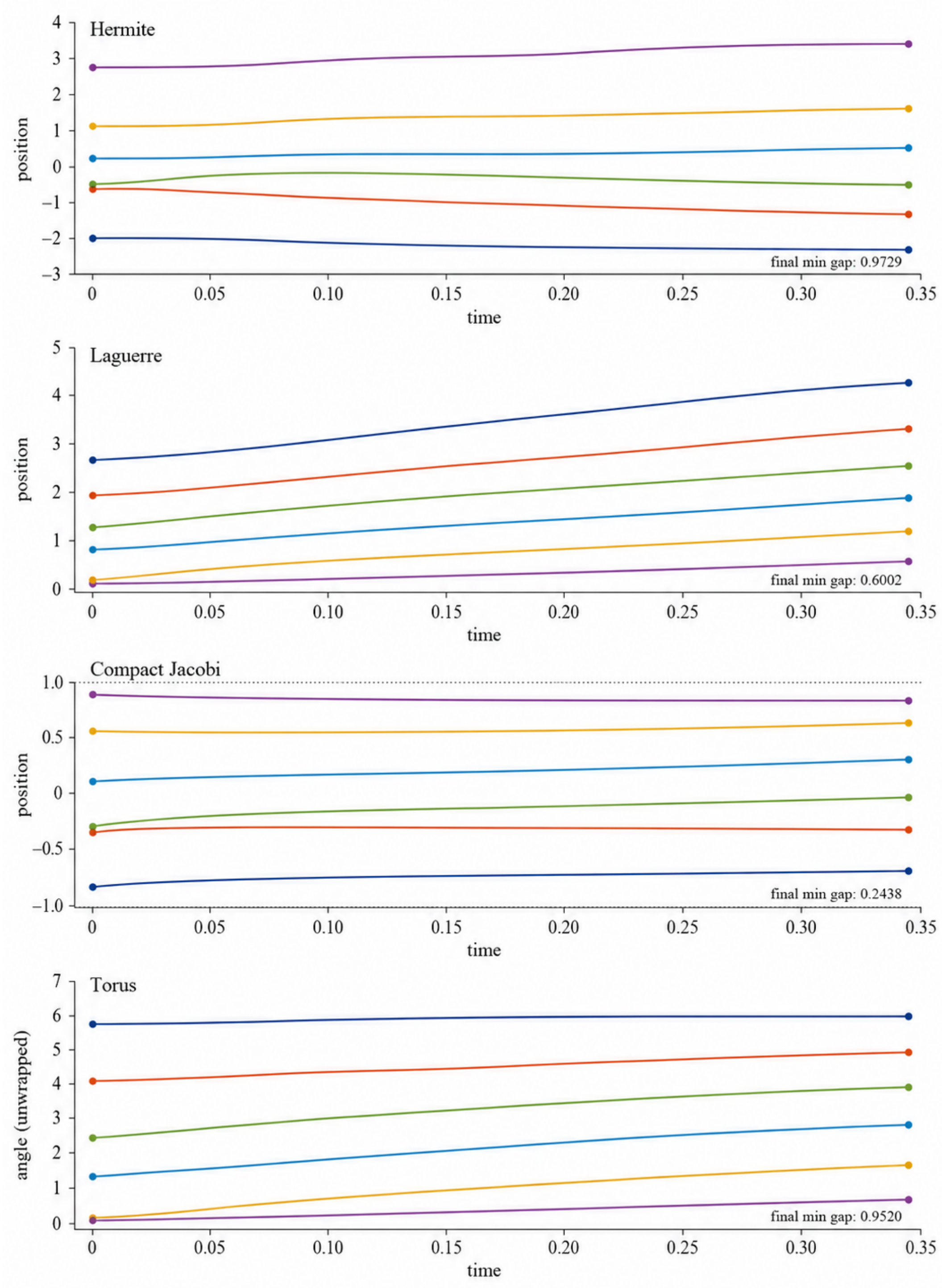

Figure 4: Recovered root trajectories.

The torus test case demonstrates that the polynomial parameterization in w coordinates is superior to the angular parameterization in terms of computational efficiency. The angular integration in the former case needs to account for the singularity of the cotangent due to the initial angular separation of 10^{-3}. The flow of coefficients (25), on the other hand, is diagonal. For $T = 0.35$, the recovered angular structure is

$$(0.64483363, 1.64075641, 2.71538513, 3.89577906, 5.00138576, 5.97604530). \tag{33}$$

The final minimum separation distance using the circular method is 0.9519736399. It is fairly close to the equal-spacing scale $2\pi/6 \approx 1.0472$, which was expected due to the torus convergence theorem. For this particular algorithm, 206 evaluations on the right-hand side are needed, while in case of direct integration 1466 evaluations would have been required. The evolution of the diagonal coefficients is not found analytically, since this would break the equality between adaptive-solver methods. Using the exponential form (25) would make the calculation almost costless.

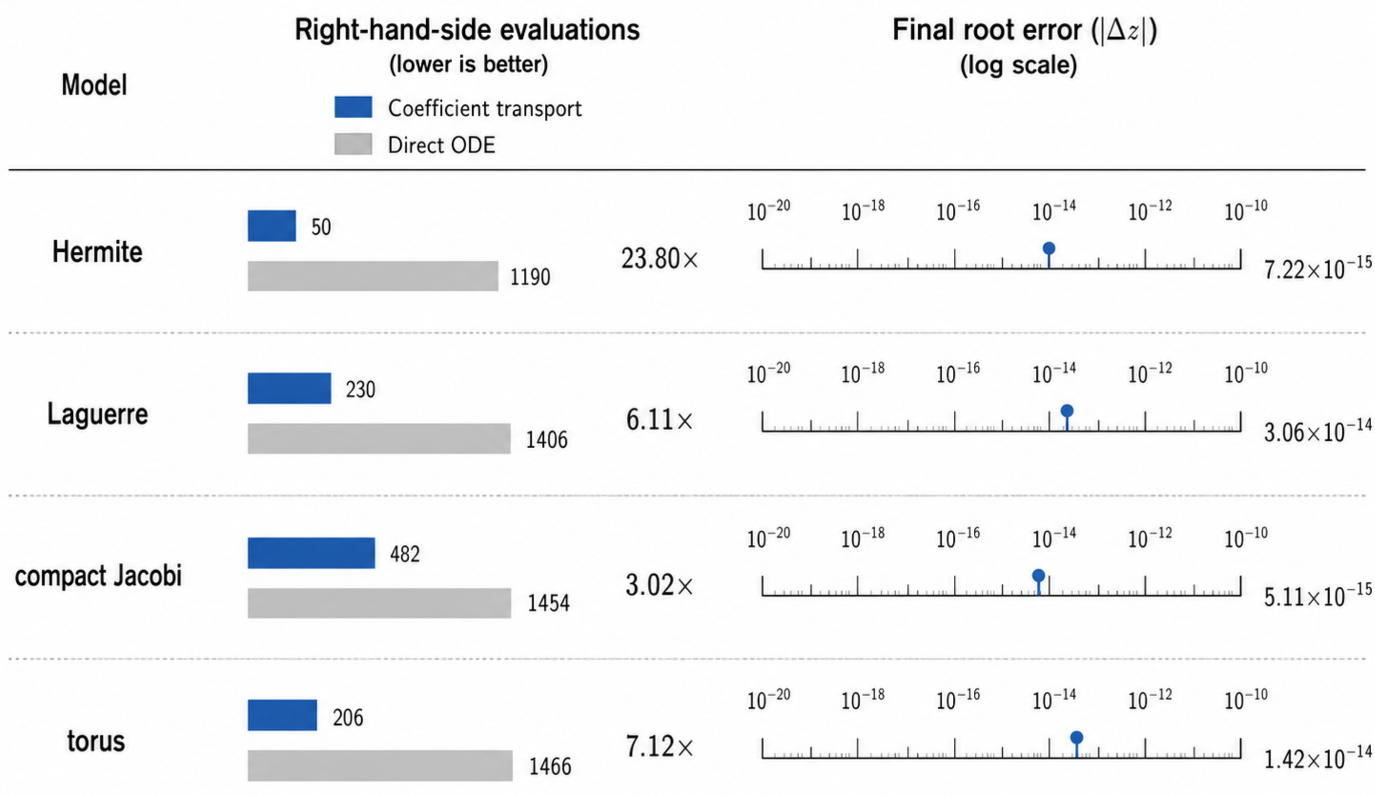

Figure 5: Cost and final root error.

The final states of Table 4 constitute the numerical data set to be subsequently interpreted. The self-similar Hermite and Laguerre final states exhibit an outward expansion, the Jacobi final state exhibits a confinement, and the torus final states are nearly regularized in circular spacing.

Table 4: Final recovered particle states.

Model	Final recovered configuration
Hermite	$(-2.88614035, -1.45135722, -0.47845925, 0.53722746, 1.69364357, 3.38558580)$
Laguerre	$(0.64680167, 1.24699982, 1.87496073, 2.55473858, 3.32824333, 4.28717256)$
Compact Jacobi	$(-0.74185867, -0.43133826, -0.07007588, 0.29690277, 0.62303130, 0.86679122)$
Torus angles	$(0.64483363, 1.64075641, 2.71538513, 3.89577906, 5.00138576, 5.97604530)$

The values of the closure residuals are presented in Table 5. The Hermite residual is exactly zero for the final state, as both the triangular recurrence and the operator evaluation involve the same floating point expression with respect to the final coefficient vector. The values for the Laguerre, compact Jacobi, and torus residuals lie between 5.70×10^{-15} and 4.44×10^{-13}. This verifies that the coefficient vectors continue to reside on the finite dimensional manifold corresponding to the operator equation. The compact Jacobi residual has the largest value due to the presence of second derivative, parameter dependent first derivative, multiplication by z and potential term in the operator; however, it is well within the bounds of not affecting the root computation accuracy.

Table 5: Closure residuals at final time.

Model	$\mathcal{R}_M(T)$
Hermite	0
Laguerre	2.36×10^{-14}
Compact Jacobi	4.44×10^{-13}
Torus	5.70×10^{-15}

Residuals presented in Table 5 confirm that the coefficient vector after transport does indeed meet the required polynomial equation. This verification process is independent of the solution of the roots using the direct solver and is mandatory since only root accuracy will not be able to catch all errors at the operator level.

For residuals, the log plot presented in Figure 6 visualizes these residuals. Along with this computation of residuals, the validation plot shown in Figure 7 shows comparison of equation-related values; i.e., radial expansion for Hermite-Laguerre case, interval margin for the compact Jacobi case, and circular gap for the torus case.

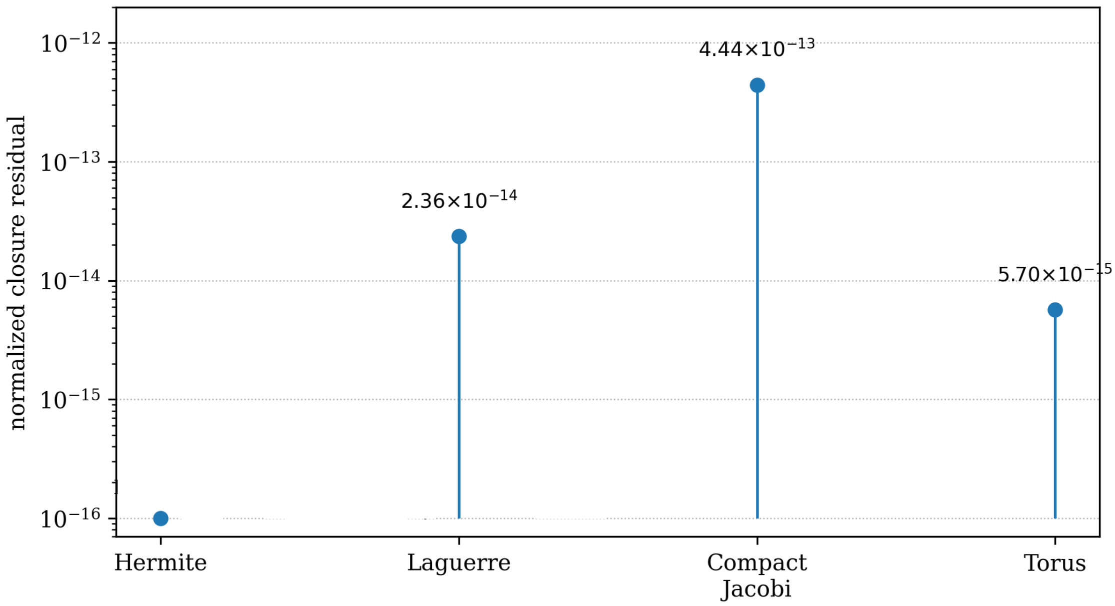

Figure 6: Operator closure residuals.

model	**quantity**	**value**	**quantity**	**value**	**check**
Hermite radius	$\|x(0)\|^2$	14.78440025	$\|x(T)\|^2$	25.28440025	identity: 25.28440025
Laguerre radius	$\|x(0)\|^2$	13.12258016	$\|x(T)\|^2$	41.47258013	identity: 41.47258016
Compact Jacobi	left clearance	0.25814133	right clearance	0.13320878	domain: $[-1, 1]$
Torus spacing	final gap	0.9519736399	regular gap	1.0471975512	ratio: 0.909068

Figure 7: Invariant and confinement checks.

The diagnostics in Figures 6 and 7 examine two separate elements of the computation. The closure residual examines the validity of the coefficient equation, whereas the invariant and confinement diagnostics check the roots found in the particle geometry.

Numerical values validate the qualitative properties derived from the equation. The Hermite and Laguerre configurations expand outward according to the norm relations (3) and (6), respectively. The Jacobi configuration is confined to $[-1, 1]$ and approaches a stationary pattern related to the zeros of the Jacobi polynomials. The torus configuration expands towards equal angular spacings while preserving the angular barycenter in the chamber convention. These geometric properties are essential since a coefficient approach might find roots with small local errors but wrong ordering or branch choice. No such error was found during computations.

Values in Table 3 demonstrate that the greatest gain is made when the vector field has a strong reciprocal singularity, but the coefficient equation is relatively sparse. The Hermite case begins with a pair of particles -0.6000 and -0.5995, which means that the vector field has a singular term of order 2.0×10^3. The corresponding coefficient equation (18) does not have any singular terms; the largest multipliers for $N = 6$ in this equation are defined by $(m + 2)(m + 1)/2$ and remain fixed integers. It is a reason for the evaluation ratio of 23.80 without any hidden fitting parameter. The final configuration of Hermite particles preserves the ordering and expands outward according to (3); the minimum separation between the particles becomes 0.9728979702.

The Laguerre case highlights a separate difficulty of the computations. The initial particles 0.1000 and 0.1004 lie close to the reflecting boundary, so both ν/x_i and $(x_i - x_j)^{-1}$, $(x_i + x_j)^{-1}$ contribute to the vector field. By squaring the coordinates, we eliminate the ambiguous signed pair and obtain the coefficient equation (21). With $\nu = 1.75$, the multipliers become $-2(m+1)(m+1.75)$, $m = 0, \ldots, 5$. In contrast to Hermite case, the stiffness depends only on the polynomial degree and not on the minimal separation between particles. The final configuration stays positive and demonstrates a smooth increase in the particle separation from the lower boundary up to the upper particles. This property is in agreement with the Bessel-like repulsion from zero and with the self-similar solution of the Laguerre equation determined by $L_N^{(\nu-1)}$.

The compact Jacobi case demonstrates the lowest evaluation ratio, but it is the most structurally complicated of all bounded cases. Parameters $p = 9.0$ and $q = 7.5$ provide endpoint repulsion and nonsymmetric drift on $[-1, 1]$. The final configuration lies inside the alcove and shows no artificial boundary overspill. The minimal separation in this case, 0.2437599247, is smaller than those of Hermite and Laguerre cases, because the length of the interval is fixed and the final configuration is a Jacobi-zero pattern, not an expanding self-similar one. The coefficients in (23) include the constants $A = 1.5$, $B = 2(5) - 16.5 = -6.5$, and $C = 6(16.5 - 6 + 1) = 69.0$; it means that the potential part of the operator is quite essential. The small closure residual in Table 5 confirms the presence of the term in question in the equation.

Finally, the torus case provides the clearest geometric validation. The angular initial configuration starts with the circular separation of 10^{-3} between the first two coordinates. By transforming the configuration to $w_j = \mathrm{e}^{\mathrm{i}x_j}$, we obtain a diagonal coefficient equation (25). Thus, the final angular configuration is obtained by calculating arguments of the roots. The final circular separation is quite close to the regular polygon one $2\pi/6$, while the angular barycenter remains preserved under the chamber convention. This result is essential since the torus roots can be computed precisely as complex numbers, but the angular ordering may be wrong. The present computation solves this problem: the roots remain precisely on the unit circle, and the circular matching yields an error of 1.42×10^{-14}.

7. Model-specific interpretation

It is seen from the results that the coefficient-space evolution naturally corresponds to the inverse heat identities of the frozen Calogero–Moser–Sutherland systems. In the particle representation, the drift term is singular since the equations trace the zeros directly. In the polynomial representation, the singularity arises in the form of a removable residue at the zeros of the polynomial. After the cancellation of this residue, the dynamics of the other coefficients becomes linear. That is why RCPI can efficiently integrate the near-collision starting conditions without resolving the singular repulsion layer via many adaptive time steps.

The most efficient computation of the near-collision start is provided by the Hermite model. It is in agreement with the structure of the corresponding inverse heat equation. The Hermite coefficient dynamics form a triangular matrix with a step size of two in terms of degree. Hence, high-degree coefficients influence the low-degree ones but not vice versa. The highest-degree and the second-highest-degree coefficients do not change. Such properties make the coefficient system smooth, sparse, and weakly coupled. In contrast, the direct particle integration deals with a situation where the small denominator in the initial near-collision pair leads to a large drift and the necessity of many small steps. Therefore, the evaluation ratio of 23.80 indeed reflects a real desingularization rather than a technical benefit of the method.

The Laguerre case provides another kind of verification of the approach. It is a special one in that there is a singularity not only between the pairs but also due to the factor ν/x_i that becomes large near zero. Squared variable polynomials $Q(t, y)$ absorb this boundary singularity in a linear first-order coefficient equation. This is consistent with the correspondence of the Laguerre polynomial zeros and the squared Bessel-type variables. On the other hand, it is important from the computational point of view since it does not allow treating the root at the reflecting boundary as a usual line root. It is seen from the final configuration that there is a robust separation both from zero and from the particle that initially was close to it. The evaluation ratio is lower than in the Hermite case but is still sufficiently large.

The compact Jacobi case demonstrates the importance of endpoint geometry. There is the factor $1 - x_i x_j$ that combines the pairwise repulsion and the compact interval geometry. In the trigonometric variables $x_i = \cos\tau_i$, one can analyze convergence using the gradient structure, but the polynomial equation remains algebraic in z. Coefficient operator includes the potential term $-N(p + q - N + 1)P$ needed to ensure the preservation of polynomial degree. The potential term is not an artificial correction in the numerical sense but the one which makes the polynomial subspace finite dimensional. It is seen from the experiment that the banded coefficient system performs better than the direct integration but is not as efficient as the triangular Hermite and Laguerre flows. This order is expected since the increased algebraic coupling in the coefficient space decreases but does not eliminate the benefit of desingularization.

The interval plot in Figure 8 displays these constants along with the final root pattern. Since the endpoint asymmetry, the inward coefficient drift, and the potential term enter the compact Jacobi equation explicitly, the bounded interval computation is not a trivial Hermite-like problem.

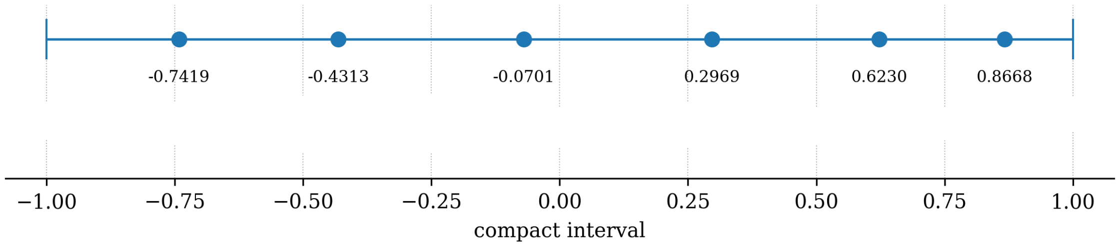

Figure 8: Compact Jacobi coefficient constants.

The torus case is conceptually different from others since the particle positions are angular, and the direct equation includes the singular cotangent interaction term. Transformation $w_j = \exp(ix_j)$ removes the trigonometric singularity and turns the polynomial coefficient dynamics into a diagonal matrix. Final angles are close to equally spaced ones, which is expected due to the known convergence of the torus particles to a regular circular arrangement. The direct solver needs the largest number of evaluations in comparison with other direct computations due to the very small initial angular separation and the steepness of the cotangent term. The coefficient-based technique completely avoids this singularity. Therefore, the torus result demonstrates that RCPI can be particularly useful for the circular ensembles and CMS systems in the complex variables representation.

The circular version of the same test is shown in Figure 9. Unit-circle roots illustrate the angular geometry explicitly, while the lower coefficient strip represents the diagonal factors driving the torus coefficient dynamics.

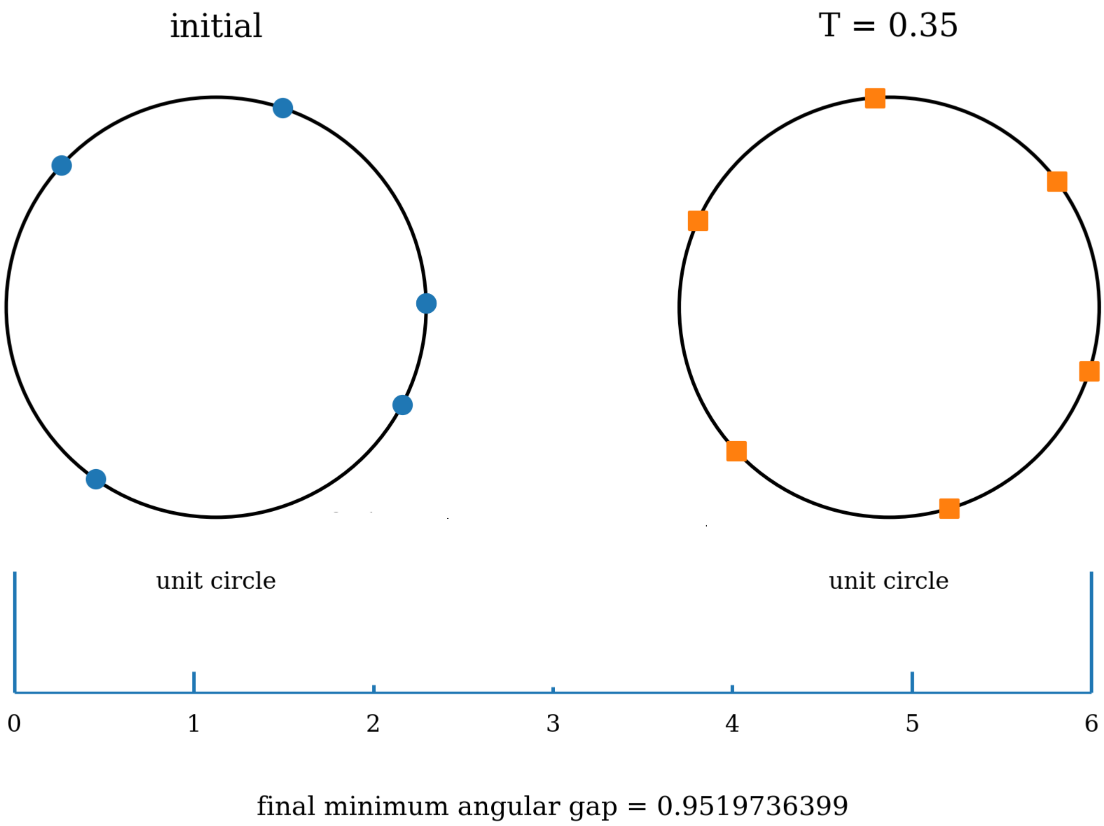

Figure 9: Torus roots and diagonal coefficient decay.

The determinantal identities provide another interpretation of the method beyond the deterministic ODE integration. Their Brownian-motion and martingale components utilize the standard continuous-process setting [31]. For the Hermite case, let us consider that $(X_{t,k})_{t\geq 0}$ is the renormalized type-A Bessel process and $(B_t)_{t\geq 0}$ is an independent one-dimensional Brownian motion. Then the polynomial identity gives

$$E\left[\prod_{i=1}^{N}\left(B_t + y - X^i_{t,k}\right)\right] = \prod_{i=1}^{N}(y - x_i). \tag{34}$$

In the Laguerre case, with a one-dimensional Bessel process Y_t of the appropriate index, the corresponding identity is

$$E\left[\prod_{i=1}^{N}\left(Y_t^2 - (X^i_{t,\nu,\beta})^2\right)\right] = \prod_{i=1}^{N}(y^2 - x_i^2). \tag{35}$$

For the compact Jacobi case, the same logic yields the exponential factor

$$E\left[\prod_{i=1}^{N}\left(Y_{t,p+N-1,q+N-1}-X^{i}_{t,\kappa,p,q}\right)\right]=\mathrm{e}^{-N(p+q-N+1)t}\prod_{i=1}^{N}(y-x_i). \tag{36}$$

From these identities, one sees that coefficient evolution agrees with the martingale structures of the stochastic processes. Thus the method can be applied not only to integrate frozen deterministic equations, but also to evaluate polynomial observables which are stable under high inverse-temperature scaling.

The determinant products in Figure 10 are written at the polynomial level. The same coefficient vector determines both the recovered roots and the polynomial observables entering the expectation identities.

Hermite	$\mathbb{E}\prod_{i=1}^{N}(B_t+y-\widetilde{X}_i(t))=\prod_{i=1}^{N}(y-x_i(0))$
Laguerre	$\mathbb{E}\prod_{i=1}^{N}(Y_t^2-\widetilde{X}_i(t)^2)=\prod_{i=1}^{N}(y^2-x_i(0)^2)$
Jacobi	$P(t,z)=\prod_{i=1}^{N}(z-x_i(t))$ under the Jacobi inverse operator
Torus	$P(t,z)=\prod_{i=1}^{N}(z-w_i(t)),\quad w_i(t)\in S^1$

Figure 10: Polynomial observables in expectation identities.

Another implication of this technique is parameter continuation. Particle-wise, varying the parameters ν, p, and q leads to the change of the singular drift and may introduce stiffness in the neighbourhood of the boundary. Coordinate-wise, the parameters enter as operator coefficients in a linear operator. Therefore, it becomes quite easy to follow the motion of the roots with varying parameters. For example, in the compact Jacobi model increasing p relative to q shifts the stationary Jacobi-zero configuration by the weights $(1-x)^{q-N}(1+x)^{p-N}$. The coefficient semigroup can be recalculated for different parameter values and root continuation can be done after the stable coefficient evolution. This way seems promising for the study of large parameter limits and free probability limits of symmetric polynomial statistics.

Moreover, the method allows us to understand why classical orthogonal polynomial zeros appear in frozen systems. In the Hermite and Laguerre models, the self-similar coefficient solutions are heat and Bessel-heat polynomials, respectively. In the compact Jacobi model, the stationary polynomial solutions are Jacobi polynomials with the parameters depending on p and q. Those are not just equilibrium markers, but invariant or asymptotically selected polynomial states under the finite-dimensional semigroup action. This interpretation fits well with Stieltjes' electrostatic interpretation of orthogonal polynomial zeros and with the modern interpretation of high inverse-temperature limits via random linear operators.

However, there are limitations. Polynomial coefficients are ill-conditioned for large N, especially in the case of clustering or wide spread roots. A particle solver suffers from the singular drift near collisions; a coefficient solver suffers from the root extraction and coefficient scaling. The best practical solver may therefore combine both techniques: use coefficient transport through singular layers and switch to the particle coordinates once the minimal separation becomes large enough or use particle coordinates for long periods of time and check the polynomial closure from time to time. One may also try to use the orthogonal polynomial bases instead of monomials. Hermite, Laguerre, or Jacobi bases may reduce the coefficient growth and ill-conditioning in high-degree tests.

The numerical experiments performed in this paper are deliberately small to make the comparison transparent. The larger systems require root conditioning, balanced companion linearizations, and multiprecision arithmetic. The results should thus be interpreted as a demonstration of the desingularization idea rather than a complete performance profile for all dimensions. Nevertheless, the evaluation reduction achieved for $N=6$ is already significant, and the method uses the algebraic structure already inherent in the frozen equations. This makes the method mathematically sound and computationally efficient.

The non-compact Jacobi model was included in the operator formulation but excluded from the numerical comparison since it requires different diagnostics from the compact models. Namely, there is no stationary zero configuration as in the compact Jacobi case. A proper numerical study would involve the comparison of the coefficient transport to the direct integration after rescaling by the natural exponential growth rate. One would also need to monitor the root ordering in the unbounded chamber. That extension is conceptually simple but needs a separate discussion since the conditionality of the large positive roots differs from the conditionality of roots in compact intervals.

The Hermite theory also connects the inverse heat equation with real zeros under the heat flow. The Lehmer-pair analysis relates the zero spacing to the de Bruijn-Newman constant and the Riemann hypothesis [32]. Later, it was proven that the de Bruijn-Newman constant is non-negative [33]. The recent works on the heat flow extend the perspective to Gaussian analytic functions and random-polynomial setting [34]. The current method does not touch these infinite-dimensional problems. Nevertheless, the method provides a finite-dimensional computational analogy: the real-rootedness is preserved along the coefficient flow if the initial polynomial corresponds to an admissible ordered particle state. The method is therefore useful for the numerical study of finite-dimensional approximations of real-zero heat-flow problems.

The comparison demonstrates also an organizing principle for the computational papers on singular interacting particles. The direct solver may be used as a reference, but should not be the only representation of the problem. If a polynomial closure is available, the manuscript should include the root equation, the polynomial equation, the finite-dimensional coefficient system, and the validation quantity in the same mathematical normalization. This avoids the common mistake of presenting the stochastic process, frozen ODE, and the numerical implementation in incompatible scalings. In the current paper, the inverse temperature scaling is already absorbed into the frozen ODEs and the coefficient systems are obtained from them without changing time units. This is the reason why the comparison can be interpreted consistently for the Hermite, Laguerre, Jacobi, and torus models.

Also, it should be noted that the coefficient transport should not be presented as a black-box numerical acceleration. Its advantage comes from the algebraic properties of the model. In the Hermite case the second derivative in the inverse heat equation lowers the degree by two. In the Laguerre case the Bessel operator in the squared variable lowers the degree by one. In the compact Jacobi case the second derivative, first derivative, multiplication by z, and potential term together preserve the degree. In the torus case the Euler-type operator acts diagonally on monomials. All these observations not only explain the order of computational difficulty, but also prove that the method is not automatically available for every singular particle system. Indeed, a model without degree-preserving operator would need different basis, truncation argument, or another analytic transform.

The significance of classical orthogonal polynomials also becomes evident from the experiments. Generalized classical polynomials allow a direct algebraic transition to the Calogero-Sutherland model [35]. Jack symmetric functions provide a similar combinatorial structure for multivariate polynomial systems [36]. Their large-variable asymptotics extend the connection between symmetric polynomials and the limiting particle behaviour [37]. From the particle perspective, Hermite, Laguerre, and Jacobi zeros are the special configurations which solve the equilibrium or self-similar balance equations. From the semigroup perspective, they are the polynomial modes which are selected by the inverse operators. Both interpretations are equivalent and emphasize different aspects of the problem. The particle interpretation is geometrical and electrostatic and follows the Stieltjes tradition. The coefficient interpretation is operator-theoretical and computational. A good manuscript on frozen Calogero-Moser-Sutherland dynamics should therefore keep both perspectives in mind since the analytical proofs often rely on the former while the stable computation relies on the latter.

The computed values also hint how the method could be scaled in practice. For moderate N, coefficient transport followed by the root extraction becomes attractive because of the small size of the linear system and manageable root problem. For large N, the direct root extraction from the monomial coefficients could become the bottleneck. This means that the coefficient representation should be used together with numerically stable polynomial bases or companion linearizations. Orthogonal bases appropriate for the model such as Hermite, Laguerre, or Jacobi bases may reduce the coefficient growth and ill-conditioning. In the torus case, the Fourier or elementary symmetric representations may be more stable than the monomials. These are just the implementation refinements which preserve the key idea of desingularizing the time evolution before root extraction.

Finally, the determinant identities with respect to the inverse heat operators should be discussed in connection with the method. In the Hermite model, the Brownian motion evaluated inside the polynomial generated by the frozen roots is a time-independent process giving the expectation equal to the initial polynomial. In the Laguerre model, the corresponding process is the one-dimensional Bessel process with the index $\nu + 1/(2\beta) - 1$, and the identity involves $Y_t^2 - (\widetilde{X}^i_{t,\nu,\beta})^2$. In the compact and non-compact Jacobi models, the one-dimensional Jacobi process with shifted parameters $p + N - 1$ and $q + N - 1$ and the potential factor $\exp\{N(p + q - N + 1)t\}$ are involved in the non-compact expectation. In the torus model, the corresponding factor is the complex geometric Brownian expression used with the unit-circle polynomial. The coefficient method preserves the same polynomial quantities because it advances exactly the polynomial whose elementary symmetric coefficients are involved in the expectations. This is why the method is not just a root tracker but a polynomial operator computation of the quantity entering the martingale and expectation formulas.

The computations also show that the method separates time evolution from root recovery. The direct particle integration unites these two tasks because the solver evaluates the singular drift at each step. Coefficient transport performs the time evolution in a nonsingular finite-dimensional space and postpones the root recovery until output times. This separation is beneficial if the trajectories are needed at a relatively small number of observation times. If a dense history of the trajectories is needed, the root recovery can be done at each requested time or the recovered roots can be polished by the Newton correction using the previous observation as the starting value. In this case, the polynomial residual (28) will provide a direct verification that the recovered roots correspond to the solution of the correct inverse operator equation.

As for high-degree systems, the monomial basis should be chosen with care. The current six-particle calculations are deliberately small enough that the monomial coefficients and root extraction remain reliable. For larger systems, the coefficient growth will be strong, especially for Laguerre and Jacobi polynomials with large endpoint parameters. A stable implementation will then require the scaled monomials, orthogonal polynomial bases, or companion linearizations respecting the recurrence. These modifications will not change the mathematical content of the method: the Hermite operator will still lower the degree by two, the Laguerre operator will still lower the degree in the squared variable by one, the Jacobi operator will still preserve the degree combining second-order and first-order pieces with the potential term, and the torus operator will still act diagonally on monomials. They will only improve the numerical conditioning.

The method is therefore most helpful when the singular layer is the dominant computational difficulty. It is less useful when the particle coordinates are already well separated and only a small number of particles are involved since the direct integration will be cheap while the root recovery may dominate the cost. Its strongest use cases are the boundary starts, near-collision initialization, parameter continuation in ν, p, and q, and the computation of polynomial expectations. In these cases, the explicit coefficient Eqs. (18), (21), (23), (24), and (25) give a reproducible recipe for transforming the frozen CMS equations to the stable numerical states.

The coefficient equations also provide a transparent explanation of parameter dependence. In the Laguerre case, the change of ν implies the change of the factors $m+\nu$ in (21); therefore, the stronger repulsion from zero is immediately seen in the lower-degree coefficients of $Q(t,y)$. In the compact Jacobi case, the endpoint asymmetry enters as $A=p-q$, the global inward drift as $B=2(N-1)-(p+q)$, and the potential term as $C=N(p+q-N+1)$. For the numerical values $N=6$, $p=9.0$, and $q=7.5$, the constants are $A=1.5$, $B=-6.5$, and $C=69.0$. These values explain why the compact Jacobi coefficient equation is not so sparse as the Hermite and Laguerre recurrences. Also, one sees that the endpoint effects are not hidden behind any tuning parameter, but explicitly entered in the coefficient equation solved.

The non-compact Jacobi equation is included even though the comparison of numerical methods involves the compact interval model. The inclusion is mathematically useful since it tests whether the coefficient representation is tied to the compactness or the algebraic properties of the drift. Equation (24) shows that the same polynomial idea holds if $1-z^2$ is replaced by z^2-1 and the sign structure of the drift is reversed. This change of the drift makes the dynamics diverge from the stationary vector of zeros on a bounded interval. This is precisely why the paper describes the non-compact case by the operator equation and expectation identity and not by the same final-time comparison table. The coefficient relation stays true but the qualitative interpretation changes.

The torus case provides a complementary lesson. In angular variables, the singularity is trigonometric and the drift involves the cotangents. After the transformation $w_j=\mathrm{e}^{\mathrm{i}x_j}$, the polynomial coefficients evolve through the diagonal equation (25). The coefficient $a_m(t)$ is multiplied by $\exp\{m(m-N)t\}$ if the diagonal flow is evaluated exactly. This makes the torus computation structurally different from the line and interval cases: the finite-dimensional operator does not couple adjacent coefficients. The numerical comparison, however, uses the same adaptive procedure as the other tests to make the evaluation counts comparable. The resulting factor of reduction 7.12 is therefore conservative compared to what an exact diagonal update would achieve.

Finally, the coefficient method reveals the structure of the proof in the computation. The root equations involve the residues at $z=x_i(t)$ or $z=w_i(t)$, while the polynomial equations only involve the derivatives of P or Q. The equivalence proof is the precise cancellation of these residues. The numerical procedure mirrors the proof by never computing the singular residues during time stepping. This is the main reason why the method stays stable at the boundary start since the singularity is present in the root coordinates but is already cancelled in the polynomial coefficients. For the manuscript presentation, this correspondence between the proof and the computation is crucial since it transforms the numerical acceleration to a mathematically constrained algorithm.

The numerical tolerances used here also need an interpretation. The absolute tolerance 10^{-14} and relative tolerance 10^{-12} are stricter than the accuracy required to observe the qualitative separation of the particles. They were chosen because the coefficient and particle calculations solve the same deterministic dynamics in different coordinates, so the discrepancy should be limited by the floating-point arithmetic and root extraction. The resulting errors confirm this expectation: in all four computed cases, $E_\infty(T)$ is at least two orders of magnitude smaller than the relative tolerance and never exceeds

3.06×10^{-14}. Such a small difference would be impossible if some drift term, endpoint parameter, potential factor, or circular matching convention was missed.

The tables also reveal the time scale. The choice $T = 0.35$ is long enough for the near-collision pair to separate in each computed model, but not so long that every system reaches its limiting configuration. This is necessary for the comparison of the methods. If T was very small, the direct integration would mostly reflect the singular start; if T was very large, the self-similar expansion or the stationary attraction could dominate the numerical picture. At $T = 0.35$, the computations still retain the model-specific features: the Hermite and Laguerre states expanded, the compact Jacobi state remained in the interval with unequal endpoint distances, and the torus state moved considerably towards the equal angular spacing without reaching it.

8. Conclusion

The Hermite, Laguerre, compact Jacobi, and torus computations verify the key statement of the paper at the specified parameters. The near-collision frozen CMS trajectory can be evolved in the coefficient space, recovered as a root configuration, and checked against the particle geometry without recomputation of the singular pairwise drift. At $N = 6$ and $T = 0.35$, the four final root errors range from 5.11×10^{-15} to 3.06×10^{-14}, the closure residuals are at roundoff level, the Hermite and Laguerre squared-radius identities are satisfied, the compact Jacobi roots remain in $[-1, 1]$, and the torus roots reach the regular angular spacing.

The main conclusion is therefore that the singularity is a coordinate problem, not an unavoidable numerical feature of the frozen dynamics. In the root coordinates, the near-collision start gives the large reciprocal or cotangent drift terms; in the polynomial coordinates, the same terms are already cancelled as residues and the finite-dimensional coefficient system is nonsingular. This explains the dependence of the evaluation reduction on the coefficient operator: the Hermite triangular recurrence gives the largest gain, the Laguerre squared-variable recurrence gives a substantial gain, the compact Jacobi banded operator gives a smaller but still noticeable gain, and the torus diagonal flow gives a geometry-specific gain which would be even larger if it was evaluated by its exact exponential form.

The method is best considered as a certified polynomial computation, not just as a faster ODE solver. Its output includes the final roots, closure residuals, invariant checks, and model-specific geometric validation. For larger particle numbers, the same method should be combined with better-conditioned polynomial bases or structured root solvers, but the conclusion of the current study is already evident: residue-cancelled polynomial integration provides the reliable near-collision route for the frozen CMS systems whenever the inverse operator preserves the polynomial degree.

Conflict of interest

The author declares no conflict of interest.

References

[1] Calogero, F. (1971). Solution of the one-dimensional N-body problems with quadratic and/or inversely quadratic pair potentials. Journal of Mathematical Physics, 12(3), 419-436.
[2] Sutherland, B. (1971). Exact results for a quantum many-body problem in one dimension. Physical Review A, 4(5), 2019.
[3] Dyson, F. J. (1962). A Brownian-motion model for the eigenvalues of a random matrix. Journal of Mathematical Physics, 3(6), 1191-1198.
[4] Rogers, L. C., & Shi, Z. (1993). Interacting Brownian particles and the Wigner law. Probability theory and related fields, 95(4), 555-570.
[5] Dunkl, C. F. (1989). Differential-difference operators associated to reflection groups. Transactions of the American Mathematical Society, 311(1), 167-183.
[6] Rösler, M. (1998). Generalized Hermite polynomials and the heat equation for Dunkl operators. Communications in Mathematical Physics, 192(3), 519-542.
[7] Rösler, M., & Voit, M. (1998). Markov processes related with Dunkl operators. Advances in Applied Mathematics, 21(4), 575-643.
[8] Yor, M., Chybiryakov, O., & Gallardo, L. (2008). Dunkl processes and their radial parts relative to a root system. Harmonic and stochastic analysis of Dunkl processes, 113-197.
[9] Forrester, P. J. (2010). Log-gases and random matrices (LMS-34). Princeton university press.
[10] Katori, M. (2016). Bessel processes, Schramm-Loewner evolution, and the Dyson model (Vol. 11). Singapore: Springer.
[11] König, W., & O'Connell, N. (2001). Eigenvalues of the Laguerre process as non-colliding squared Bessel processes.
[12] Demni, N. (2009). Beta Jacobi processes. arXiv preprint arXiv:0901.0324.
[13] Anderson, G. W., Guionnet, A., & Zeitouni, O. (2010). An introduction to random matrices (No. 118). Cambridge university press.
[14] Andraus, S., Katori, M., & Miyashita, S. (2012). Interacting particles on the line and Dunkl intertwining operator of type A: application to the freezing regime. Journal of Physics A: Mathematical and Theoretical, 45(39), 395201.
[15] Andraus, S., Katori, M., & Miyashita, S. (2014). Two limiting regimes of interacting Bessel processes. Journal of Physics A: Mathematical and Theoretical, 47(23), 235201.
[16] Cépa, E., & Lépingle, D. (1997). Diffusing particles with electrostatic repulsion. Probability theory and related fields, 107(4), 429-449.
[17] Graczyk, P., & Małecki, J. (2014). Strong solutions of non-colliding particle systems.
[18] Michael, V. O. I. T., & Woerner, J. H. (2022). The differential equations associated with Calogero-Moser-Sutherland particle models in the freezing regime. Hokkaido Mathematical Journal, 51(1), 153-174.
[19] Voit, M. (2025). On the differential equations of frozen Calogero-Moser-Sutherland particle models. Journal of Mathematical Analysis and Applications, 541(2), 128710.

[20] Dumitriu, I., & Edelman, A. (2005). Eigenvalues of Hermite and Laguerre ensembles: large beta asymptotics. In Annales de l'IHP Probabilités et statistiques (Vol. 41, No. 6, pp. 1083-1099).
[21] Andraus, S., & Voit, M. (2019). Limit theorems for multivariate Bessel processes in the freezing regime. Stochastic Processes and their Applications, 129(11), 4771-4790.
[22] Voit, M. (2019). Central limit theorems for multivariate Bessel processes in the freezing regime. Journal of Approximation Theory, 239, 210-231.
[23] Kornyik, M., Voit, M., & Woerner, J. (2021). Some martingales associated with multivariate Bessel processes. Acta Mathematica Hungarica, 163(1), 194-212.
[24] Auer, M., Voit, M., & Woerner, J. H. (2024). Wigner-and Marchenko–Pastur-Type Limit Theorems for Jacobi Processes. Journal of Theoretical Probability, 37(2), 1674-1709.
[25] Voit, M. (2023). Freezing limits for Calogero–Moser–Sutherland particle models. Studies in Applied Mathematics, 151(4), 1230-1281.
[26] Szeg, G. (1939). Orthogonal polynomials (Vol. 23). American Mathematical Soc..
[27] Hirsch, M. W., Devaney, R. L., & Smale, S. (1974). Differential equations, dynamical systems, and linear algebra (Vol. 60). Academic press.
[28] Heckman, G., & Opdam, E. M. (2021). Jacobi polynomials and hypergeometric functions associated with root systems. Encyclopedia of Special Functions, Part II: Multivariable Special Functions, eds. TH Koornwinder, JV Stokman, Cambridge University Press, Cambridge.
[29] Schapira, B. (2007). The Heckman–Opdam Markov processes. Probability theory and related fields, 138(3), 495-519.
[30] Hobson, D. G., & Werner, W. (1996). Non-colliding Brownian motions on the circle. Bulletin of the London Mathematical Society, 28(6), 643-650.
[31] Revuz, D., & Yor, M. (2013). Continuous martingales and Brownian motion. Springer Science & Business Media.
[32] Csordas, G., Smith, W., & Varga, R. S. (1994). Lehmer pairs of zeros, the de Bruijn-Newman constant , and the Riemann hypothesis. Constructive Approximation, 10(1), 107-129.
[33] Rodgers, B., & Tao, T. (2020, January). The de Bruijn–Newman constant is non-negative. In Forum of Mathematics, Pi (Vol. 8, p. e6). Cambridge University Press.
[34] Hall, B., Ho, C. W., Jalowy, J., & Kabluchko, Z. (2023). The heat flow, GAF, and SL (2; R). arXiv preprint arXiv:2304.06665.
[35] Baker, T. H., & Forrester, P. J. (1997). The Calogero-Sutherland model and generalized classical polynomials. Communications in Mathematical Physics, 188(1), 175-216.
[36] Stanley, R. P. (1989). Some combinatorial properties of Jack symmetric functions. Advances in Mathematics, 77(1), 76-115.
[37] Okounkov, A., & Olshanski, G. (1997). Asymptotics of Jack polynomials as the number of variables goes to infinity. arXiv preprint q-alg/9709011.